*Manuscript (Text only)
Click here to view linked References

Submitted to *Scripta Materialia*, September 2019. Revised October 2019.

Highly sliding-wear resistant B_4C composites fabricated by spark-plasma sintering with Ti-Al additives

Angel L. Ortiz [a,*], Carlos A. Galán [b], Oscar Borrero-López [a], Fernando Guiberteau [a]

[a] Departamento de Ingeniería Mecánica, Energética y de los Materiales, Universidad de Extremadura, 06006 Badajoz, Spain.

[b] Departamento de Física Aplicada, Universidad de Extremadura, 06006 Badajoz, Spain.

Abstract

The lubricated sliding-wear resistance of a fine-grained B_4C composite fabricated by transient liquid-phase assisted spark-plasma sintering with Ti-Al additives at smooth conditions is critically compared to that of its reference monolithic B_4C ceramic. It is shown that the former has an excellent sliding-wear resistance that exceeds that of the later by one order of magnitude (far less specific wear rate, worn volume, and wear damage), attributable to its greater hardness and densification. The wear mode is abrasion dominated by plastic deformation, plus localized microfracture in the monolithic ceramic. Implications for fabricating highly wear-resistant tribocomponents based on superhard ceramics are presented.

Keywords: B_4C; superhard materials; wear; spark-plasma sintering; transient liquid-phase sintering.

* Corresponding author:

Angel L. Ortiz
Phone: +34 924289600 Ext: 86726
Fax: +34 924289601
E-mail: **alortiz@unex.es**

B_4C has been receiving great attention lately for the fabrication of superhard, ultra-lightweight advanced ceramics for many structural applications, and especially for the production of personnel/vehicle ballistic armours and a myriad of tribocomponents [1-10]. Unfortunately however, B_4C is hardly at all densifiable in the pure state by conventional solid-state sintering due to the kinetics limitations imposed by the strong covalent bonding and low self-diffusion coefficients, as well as by the oxidic impurities (i.e., B_2O_3 or H_3BO_3) favouring coarsening over densification [4,11]. The undesirable consequence is that monolithic B_4C ceramics are generally porous to a greater or lesser extent, and are therefore softer and weaker than expected –handicaps that in practice limit their potential in structural applications. It is then understandable that conventional liquid-phase sintering has often been used palliatively to consolidate B_4C [4]. However, liquid-phase sintering is not entirely satisfactory either because the residual intergranular phase irremediably degrades the hardness and refractoriness of the resulting B_4C composites [4].

Interestingly, it has very recently been demonstrated that it is possible to fabricate at moderate temperatures superhard, toughened, ultra-lightweight B_4C composites with triplex-particulate microstructures by spark-plasma sintering (SPS) using Ti-Al intermetallic additives [12]. Ti-Al sintering aids have also been used to fabricate B_4C composites by both hot-pressing [13] and pressureless SPS [14]. This is because the Ti-Al intermetallic promotes the transient liquid-phase sintering of B_4C, first melting to help in the densification and then reacting with part of B_4C to form in-situ TiB_2 and Al_3C_4 particles at grain boundaries and multigrain joints [12]. This is therefore an appealing and promising manner of circumventing the common drawbacks of both the solid-state sintering and liquid-phase sintering of B_4C, and merits complementary research effort. The present work was aimed in this direction, and was undertaken with the main

objective in mind of evaluating for the very first time the sliding-wear resistance of these SPS-ed B_4C composites compared to that of the corresponding reference monolithic B_4C ceramics fabricated under the same SPS conditions. This type of comparative study is of primary importance for those superhard/ultrahard ceramics that, as in the case of B_4C, are or may become very demanded for tribological applications requiring long-term durability, with the use of the same SPS cycle being essential and therefore imposed here to elucidate the true potential of the Ti-Al additives in making highly wear-resistant B_4C tribocomponents at smoother sintering conditions. In addition, evaluating the sliding wear of these advanced triboceramics is particularly relevant because this contact condition is commonly encountered in myriad applications, such as manufacturing-equipment components, dies, channels, bearings, seals, valves, etc. Finally, as an added value, the present study also seeks to complement a previous processing study with the so-far unreported analysis of the shrinkage rate curves logged during SPS to further support the densification mechanism proposed for these B_4C composites [12].

The starting materials were commercially available submicrometre B_4C (d_{50}~0.5 μm; Grade HD 20, H.C. Starck, Germany) and micrometre Ti-Al (d_{50}~40 μm; TiAl, -325 mesh, Alfa Aesar, Germany) powders. The B_4C powder contains B_4C plus impurities of C and H_3BO_3, while the Ti-Al powder contains γ-TiAl (major phase), α_2-Ti_3Al (minor phase), and $TiAl_2$ (minor phase). The two powders were then combined in a B_4C:Ti-Al wt.% ratio of 95:5, and the powder mixture was ball-milled in methanol for 24 h. Methanol was used as liquid medium to eliminate the oxidic impurities in the B_4C powder, as demonstrated elsewhere [15,16]. Moreover, this specific composition with 5 wt.% Ti-Al additive was chosen on the basis of an earlier processing study showing the optimization of the mechanical properties (hardness, toughness, and strength) of the resulting B_4C composites [12]. The slurry was subsequently dried under continuous

agitation, and the resulting dried powder mixture was finally deagglomerated. The B_4C starting powder was also methylated and dried under identical conditions to those of the B_4C+5 wt.%Ti-Al powder mixture, and used to fabricate a reference monolithic B_4C ceramic. Next, the methylated B_4C powder and the B_4C+5wt.%Ti-Al powder mixture were individually loaded into graphite dies lined with graphite foils and surrounded by graphite blankets, and both were then SPS-ed (HP D 10, FCT Systeme GmbH, Germany) in dynamic vacuum (i.e., ~3 Pa) at 1800 °C (100 °C/min heating ramp) for 5 min under 50 MPa (applied at 300 °C). After completion of the SPS cycle, the load was released and the electrical power was shut off to allow rapid cooling (in 1-2 min) to room temperature. The two resulting materials (discs of 2-cm diameter and 1-cm thickness) were ground and diamond polished to a 1-µm finish, and then characterized microstructurally by X-ray diffractometry (XRD; D8 Advance, Bruker AXS, Germany) and scanning electron microscopy (SEM; Quanta 3D, FEI, The Netherlands).

Fig. 1 shows representative SEM images (both polished and fracture surfaces) and the XRD patterns, of both the reference monolithic ceramic and the composite fabricated in the present study by SPS under the same conditions without and with Ti-Al additives, respectively. There are evident microstructural differences between them. In particular, Figs. 1A, 1C, and 1E show that the reference monolithic ceramic has a fine-grained (< 1 µm), porous (~10%; absolute density of ~2.26 g/cm^3) microstructure with only B_4C plus some residual graphite (the only impurity present in the B_4C powder purified in methanol). This corroborates the poor solid-state sinterability of pure B_4C, even under SPS. The residual porosity of this reference monolithic ceramic is responsible for its low hardness of only 18.9±0.6 GPa [12,17], as measured here experimentally by Vickers indentation tests (MV-1, Matsuzawa Seiki Co., Japan) at both 9.8 and 49 N using standard procedure and formula [18,19]. As observed in Figs. 1B, 1D, and 1F, the

composite is however essentially dense (absolute density of ~2.59 g/cm^3), and has a more complex fine-grained (~0.7-0.8 μm) microstructure with secondary phases located at both grain boundaries and multigrain joints (as demonstrated by transmission electron microscopy (TEM) elsewhere [12]). It contains B_4C and some graphite, plus TiB_2, Al_4C_3, TiO_2, and Al_2O_3 as other minor phases, but not γ-TiAl, α_2-Ti_3Al, or $TiAl_2$ used as sintering additives. It is therefore not a cermet (i.e., ceramic grains embedded into a metallic matrix), but a multi-particulate ceramic composite with a superhardness of 32.9±0.7 GPa (as also measured by Vickers indentation tests).

The processing of B_4C composites by SPS with Ti-Al additives has been studied elsewhere [12], demonstrating by a thorough microstructural characterization that densification occurs by transient liquid-phase sintering [12]. This is consistent with the present study on other B_4C starting powder (with finer particle size) with nominally the same Ti-Al additive. Besides these microstructural observations, the so-far unused analysis of the shrinkage rate curves logged during SPS could also validate the correctness of this densification mechanism. Indeed, Fig. 2 shows that the B_4C+5wt.%Ti-Al powder mixture exhibits a distinctive peak of accelerated shrinkage rate at ~1400 °C (confirmed using a B_4C+7wt.%Ti-Al powder mixture), attributable to the formation of a liquid phase that spreads rapidly between particles, filling pores [20]. This is the expectation derived from the Ti-Al binary phase diagram [21], in particular because the temperature within the SPS die is higher than that measured by the optical pyrometer. Nonetheless, despite the formation of a liquid phase there is little grain growth by solution-reprecipitation because the Ti-Al intermetallic acts as a reactive and transient liquid-phase sintering additive, not as a permanent liquid-phase sintering additive.

Fig. 3A shows the sliding-wear curves (i.e., wear volume (*V*) *vs* sliding distance (*L*)) of both the reference monolithic ceramic and the composite fabricated by SPS and then diamond

polished to a 1-μm finish. The tribological tests (Falex multi-specimen, Faville-LeVally Corp., USA) were carried out in the ball-on-three-disks geometry under total lubrication conditions (to thus avoid friction-induced heating or triboreactions), using a commercial bearing-grade Si_3N_4 ball (NBD200, Cerbec, USA) of radius 6.35 mm as counterpart, paraffin oil as lubricant (with viscosity of 34 cSt at 40 °C), a total normal contact load of 212 N (to thus apply 50 N of normal load on each disk (flat specimen of ~3.5x3.5x2.0 mm^3)), and a rotation speed of 100 rpm (corresponding to a sliding velocity of ~0.047 m/s). The wear tests were selectively interrupted to evaluate the size of the wear scar on the reference monolithic ceramic and the composite as a function of the sliding time by optical microscopy (OM; Epiphot 300, Nikon, Japan), from which worn volumes were computed as a function of the sliding distance [22] and used to calculate the specific wear rates. It can be seen in Fig. 3A that both materials show a characteristic two-stage curve, observed in other polycrystalline ceramics [10,23-25]. In particular, an initial run-in stage, in which the wear volume quickly increases until the test specimens accommodate the rotating countersphere at a sliding distance of ~150 m, is followed by a steady-state stage. In this second stage, the wear volume increases linearly with the sliding distance. It is clear that the wear resistance of the composite is dramatically improved with respect to that of the reference monolithic ceramic. Indeed, for each value of the sliding distance, the wear volume of the composite is one order of magnitude lower than that of the reference monolithic ceramic. The wear rate calculated using the data in the steady-state stage is also significantly lower in the composite than in the reference monolithic ceramic: $(1.9\pm0.2)\cdot10^{-16}$ *vs* $(1.99\pm0.09)\cdot10^{-15}$ m^3/m. The corresponding specific wear rates are $(3.8\pm0.4)\cdot10^{-18}$ (composite) and $(4.0\pm0.2)\cdot10^{-17}$ m^3/Nm (reference monolithic), which are characteristic of materials with excellent and good wear resistance, respectively [26]. The wear and specific wear rates measured for the reference

monolithic ceramic are consistent with those reported earlier (i.e., $(1.72\pm0.17)\cdot10^{-15}$ m^3/m and $(2.9\pm0.29)\cdot10^{-17}$ m^3/Nm) for a near-fully dense (~95%) monolithic B_4C ceramic [10]. Thus, the composite exhibits a sliding-wear resistance that exceeds that of the reference monolithic ceramic by one order of magnitude (i.e., $(2.6\pm0.3)\cdot10^{17}$ *vs* $(2.5\pm0.5)\cdot10^{16}$ Nm/m^3).

The patent differences between the wear resistance of the materials observed in Fig. 3A can be clearly visualized in Fig. 3B, which compares optical micrographs of the wear scars at the conclusion of the tests. Indeed, the scar in the composite is remarkably smaller than that in the reference monolithic ceramic. Moreover, clear differences in the damage mechanisms can be observed at this level of magnification. In particular, the composite shows only seemingly superficial scratches running parallel to the sliding direction. The reference monolithic ceramic shows deeper grooves, accompanied by relatively large, dark patches (pits) indicative of in-depth material removal by grain pullout.

Fig. 4 show higher magnification details of the damage inside the wear scars. As anticipated, the damage at the microstructural scale is more severe in the case of the reference monolithic ceramic, which exhibits a larger amount of wider and deeper grooves compared to the composite. In particular, Fig. 4A shows grooves of width up to ~20 μm in the reference monolithic ceramic, along with the material porosity. The grooves appear to be relatively deep, resulting in a rough wear surface, and contain abundant debris, as observed in Fig. 4B. Inside the pitted regions, material removal (i.e., grain pullout) takes place from even deeper under the surface, and crushed particles and microcracks can be observed (Figs. 4C and D). In contrast, the worn surface of the composite appears to be quite smooth and polished, and mostly contains very superficial scratches of width ~1-5 μm (Figs. 4E-G).

The wear markings observed by OM and SEM suggest that both the reference monolithic

ceramic and the composite wear by abrasion, caused by either the asperities of the countersphere (two-body wear), and/or by dislodged particles trapped under the contact (three-body wear) [26,27]. The dominant wear mechanism is plastic deformation at the asperity/particle level, responsible for the grooves and scratches. Since the resistance to plastic deformation ultimately depends on the material hardness, the wear volume is expected to correlate inversely with hardness ($V \propto H^{-1}$) according to the classical Archard's wear law [28,29]. Thus, the superior wear resistance of the composite is largely a result of its almost twofold greater hardness compared to the reference monolithic ceramic (~33 *vs* 19 GPa). Another two factors which contribute to the higher wear resistance of the composite are its great densification and small amount of wear debris generated by grain pullout. This is because the porosity provides critical defects from which fracture can initiate, as evidenced by the larger extent of microcracking observed inside the pitted regions in the reference monolith ceramic (Figs. 4C and D), resulting in more in-depth material removal by grain pullout. The hard wear debris generated, in turn, contributes to a greater extent of third-body abrasion. Last, it is worth noting that the lubrication conditions are not expected to affect the wear mechanism, only the severity of the wear damage and rate.

An interesting final consideration is that earlier tribological studies have shown the relevance of subtle differences of densification in the wear resistance of superhard/ultrahard carbides [23,24]. In particular, it has been observed that near-fully dense monolithic ZrC ceramics have lower sliding-wear resistance than ZrC composites fully densified with $MoSi_2$ (which also acts as a transient liquid-phase sintering additive), which is indeed the same conclusion reached here for the case of B_4C triboceramics. Fabrication of these advanced triboceramics under SPS at smoother conditions (i.e., at lower temperature to minimize grain growth) without compromising their full densification (for example using transient liquid-phase

sintering additives) thus emerges as a likely generic processing guideline to make them highly sliding-wear resistant.

Acknowledgements. This work was supported by the Ministerio de Economía y Competitividad (Government of Spain) and FEDER Funds under Grant no. MAT2016-76638-R. Financial support from the Junta de Extremadura under Grant no. GR15078, also co-financed with FEDER Funds, is gratefully acknowledged as well.

References

1. F. Thevenot, J. Eur. Ceram. Soc. 6 [4] (1990) 205–225.
2. M. Chen, J.W. McCauley, K.J. Hemker, Science 299 (2003) 1563–1566.
3. H. Way, N.F. Particle, Am. Ceram. Soc. Bull. 87 [5] (2008) 20–24.
4. A.K. Suri, C. Subramanian, J.K. Sonber, T.S.R.-Ch. Murthy, Int. Mater. Rev. 55 [1] (2010) 4–40.
5. V. Domnich, S. Reynaud, R.A. Haber, M. Chhowall, J. Am. Ceram. Soc. 94 [11] (2011) 3605–3628.
6. S. Leo, C. Tallon, G.V. Franks, J. Am. Ceram. Soc. 97 [10] (2014) 3013–3033.
7. D. Hallam, A. Heaton, B. James, P. Smith, J. Yeomans, J. Eur. Ceram. Soc. 35 [8] (2015) 2243–2252.
8. B.M. Moshtaghioun, D. Gómez-García, A. Domínguez-Rodríguez, R.I. Todd, J. Eur. Ceram. Soc. 36 [16] (2016) 3925–3928.
9. S. Hayun, Am. Ceram. Soc. Bull. 96 [6] (2017) 22–29.
10. A.L. Ortiz, V.M. Candelario, O. Borrero-López, F. Guiberteau, J. Eur. Ceram. Soc. 38 [4] (12018) 1158–1163.
11. S.L. Dole, S. Prochazka, R.H. Doremus, J. Am. Ceram. Soc. 72 [6] (1989) 958–966.
12. W. Ji, R.I. Todd, W. Wang, H. Wang, J. Zhang, Z. Fu, J. Eur. Ceram. Soc. 36 [10] (2016) 2419–2426.
13. W. Zhang, L. Gao, J. Li, B. Yang, Y. Yin, Ceram. Int. 37 [3] (2011) 783–789.
14. C. Ojalvo, R. Moreno, F. Guiberteau, A.L. Ortiz, J. Eur. Ceram. Soc., in press (2019).
15. B.M. Moshtaghioun, D. Gómez-García, A. Domínguez-Rodríguez, A.L. Ortiz, J. Eur. Ceram. Soc. 36 [11] (2016) 2843–2848.

16. A.L. Ortiz, F. Sánchez-Bajo, V.M. Candelario, F. Guiberteau, J. Eur. Ceram. Soc. 37 [13] (2017) 3873–3884.
17. B.M. Moshtaghioun, D. Gómez-García, A. Domínguez-Rodríguez, R.I. Todd, J. Eur. Ceram. Soc. 36 [7] (2016) 1829–1834.
18. D.J. Green, An introduction to the mechanical properties of ceramics, Cambridge University Press, Cambridge, UK (1998).
19. B.M Moshtaghioun, A.L. Ortiz, D. Gómez-García, A. Domínguez-Rodríguez, J. Eur. Ceram. Soc. 33 [8] (2013) 1395–1401.
20. C. Ojalvo, F. Guiberteau, A.L. Ortiz, J. Eur. Ceram. Soc. 39 [9] (2019) 2862–2873.
21. J.C. Schuster, M. Palm, J. Phase Equilib. Diffus. 27 [3] (2006) 255–277.
22. S.M.Hsu, M.C.Shen, Wear 200 [1–2] (1996) 154–175.
23. D. Bertagnoli, O. Borrero-López, F. Rodríguez-Rojas, F. Guiberteau, A.L. Ortiz, Ceram. Int. 41 [10 Part B] (2015) 15278–15282.
24. E. Sánchez-González, O. Borrero-López, F. Guiberteau, A.L. Ortiz, J. Eur. Ceram. Soc. 36 [13] (2016) 3091–3097.
25. O. Borrero-López, F. Guiberteau, Y. Zhang, B.R. Lawn, J. Mech. Behav. Biomed. Mat. 92 (2019) 144–151.
26. G.W. Stachowiak, A.W. Batchelor, Engineering tribology, 3rd Edition, Elsevier Butterworth-Heinemann, Oxford, UK (2005).
27. I.M. Hutchings, Tribology: friction and wear of engineering materials, CRC Press, Boca Raton, FL, USA (1992).
28. J.F. Archard, J. Appl. Phys. 32 [8] (1961) 1420–1425.
29. E. Rabinowicz, Friction and wear of materials, John Wiley and Sons, Hoboken, NJ, USA

(1965).

Figure Captions

Figure 1. SEM micrographs of the electrochemically-etched (using 1% KOH solution at a current density of 0.05 A/cm^2 for 30 s), diamond-polished surface (to a 1-μm finish) of (A) the reference monolithic B_4C ceramic and (B) the B_4C composite, as well as of the fracture surface of (C) the reference monolithic B_4C ceramic and (D) the B_4C composite. The insets in (A) and (B) are lower magnification micrographs. The sinkholes in (B) are not pores, but regions of second phases removed by the etching process [12]. XRD patterns of the (E) reference monolithic B_4C ceramic and (F) the B_4C composite. Peak assignations are included.

Figure 2. Shrinkage rate curve logged during the SPS cycle as a function of temperature for the B_4C powder and for the powder mixtures of B_4C with 5 and 7 wt.% Ti-Al. This last was measured to merely confirm the existence of a peak of accelerated shrinkage rate in the powder mixtures of B_4C with Ti-Al.

Figure 3. (A) Wear curves for the reference monolithic B_4C ceramic and the B_4C composite. Dots are the experimental data, whereas the solid lines are included as guides to the eye. The inset shows a detailed view of the wear curve of the B_4C composite up to a sliding distance of 150 m. (B) Composition of optical images of the residual wear scars in the reference monolithic B_4C ceramic and in the B_4C composite at the end of the wear tests. The same scale bar is used intentionally to ensure the straightforward visual comparison of the wear-scar sizes.

Figure 4. SEM micrographs of the damage within the wear scar of the reference monolithic B_4C ceramic taken within the grooves at (A) moderate and (B) high magnifications, and within the pitted regions at (C) low and (D) moderate magnifications, as well as SEM micrographs of the damage within the wear scar of the B_4C composite taken at (E) low, (F) moderate, and (G) high

magnifications.

Figure1

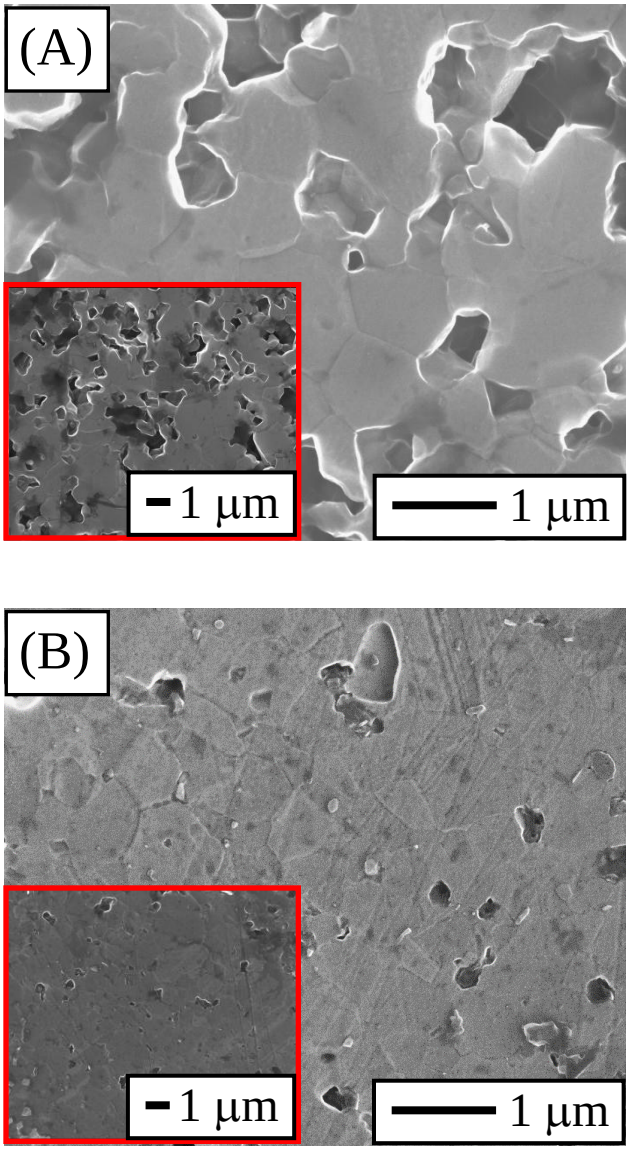

Ortiz *et al.*
Figure 1

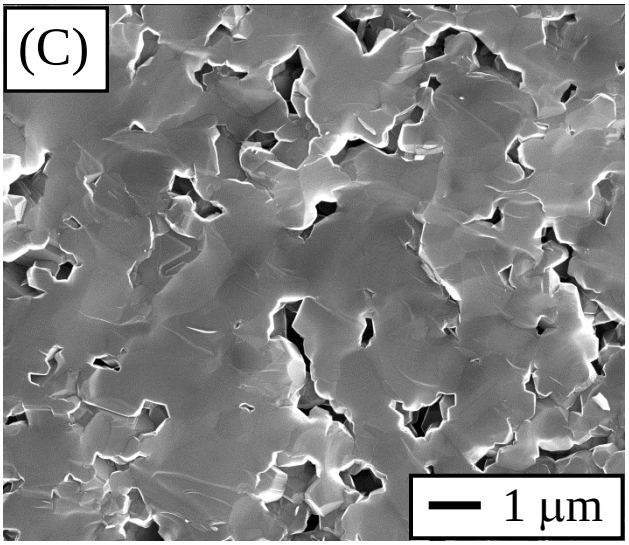

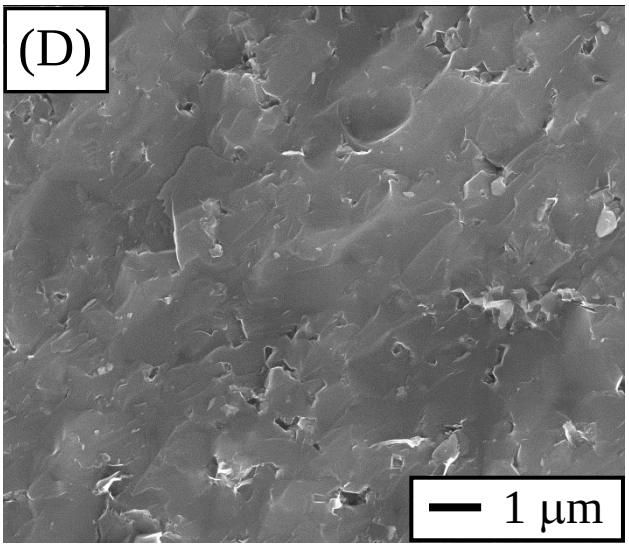

Ortiz *et al.*
Figure 1

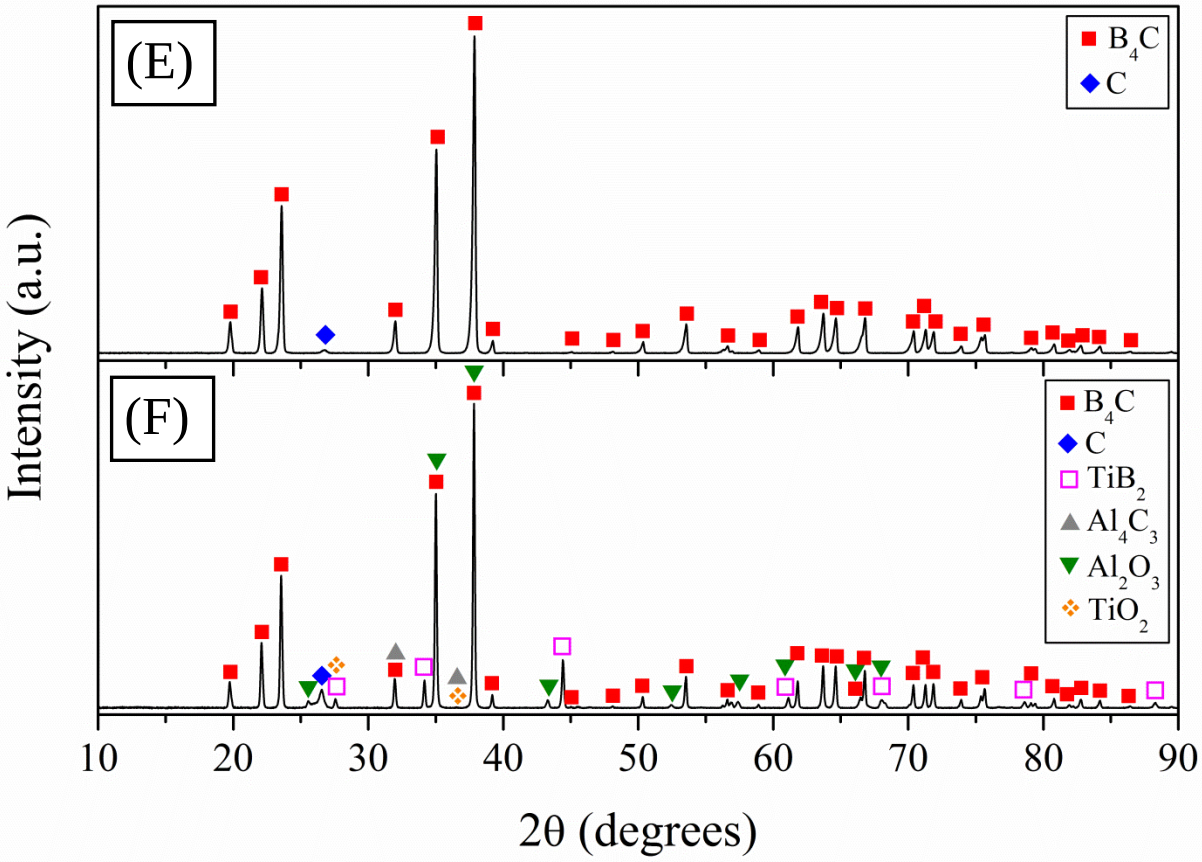

Ortiz *et al.*
Figure 1

Figure2

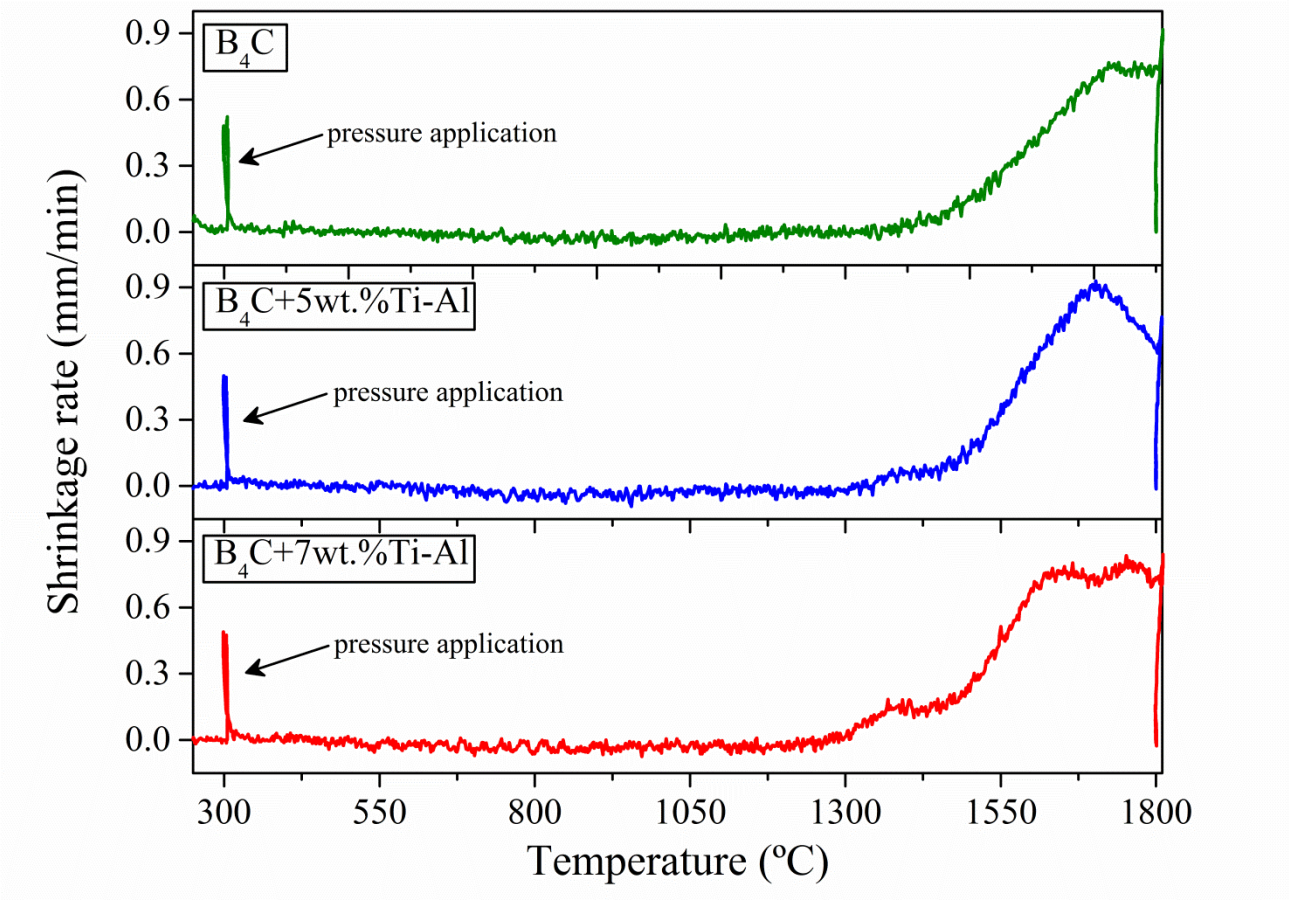

Ortiz *et al.*
Figure 2

Figure3

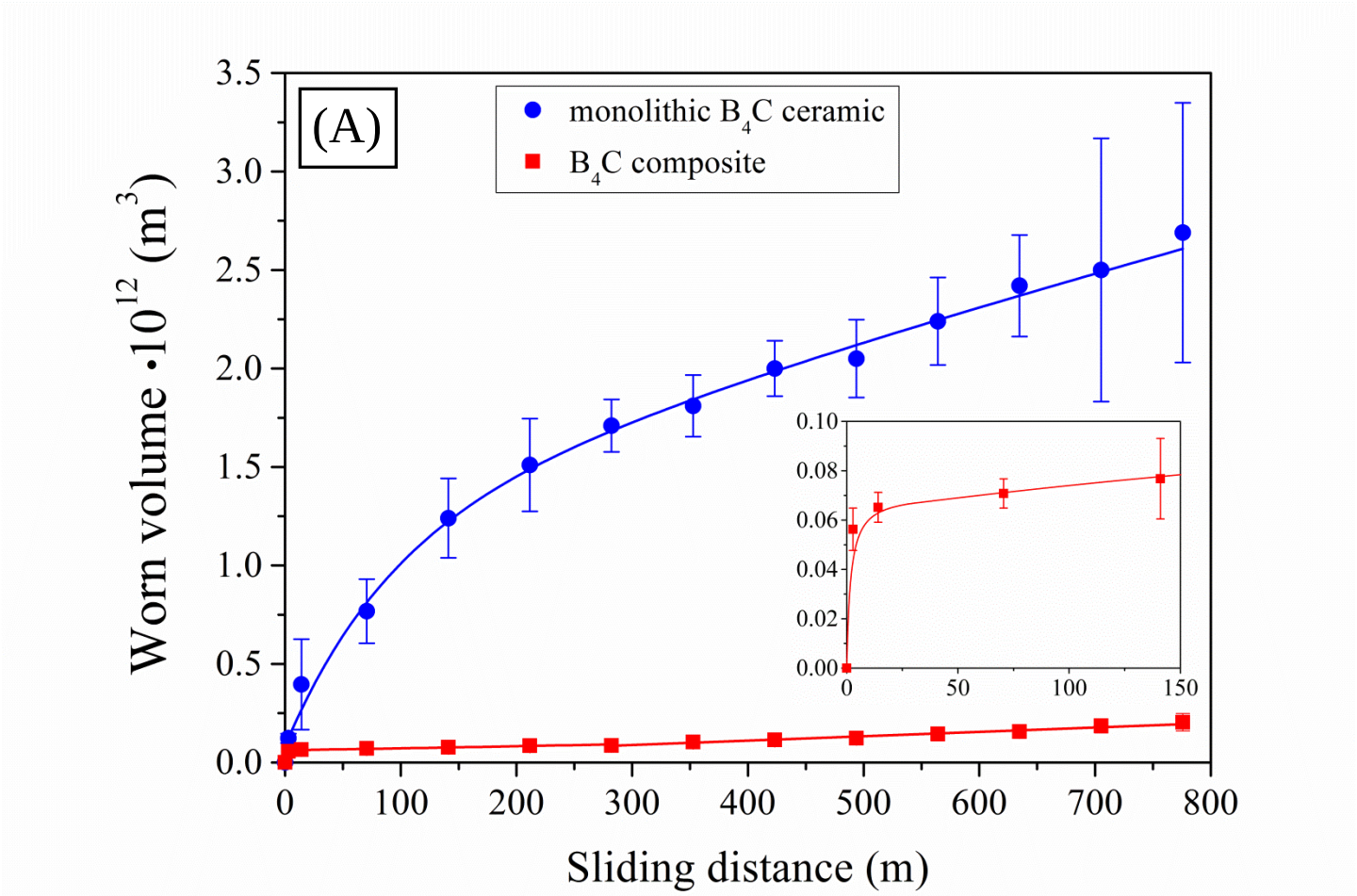

Ortiz *et al.*
Figure 3

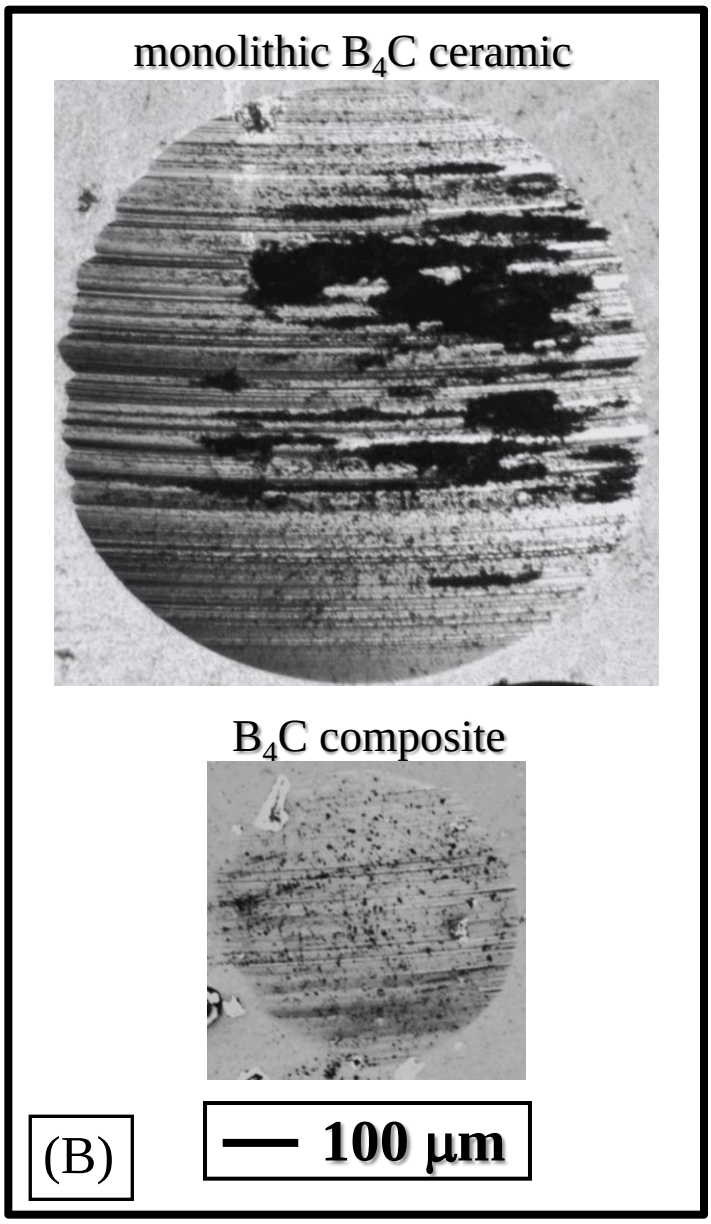

Ortiz *et al.*
Figure 3

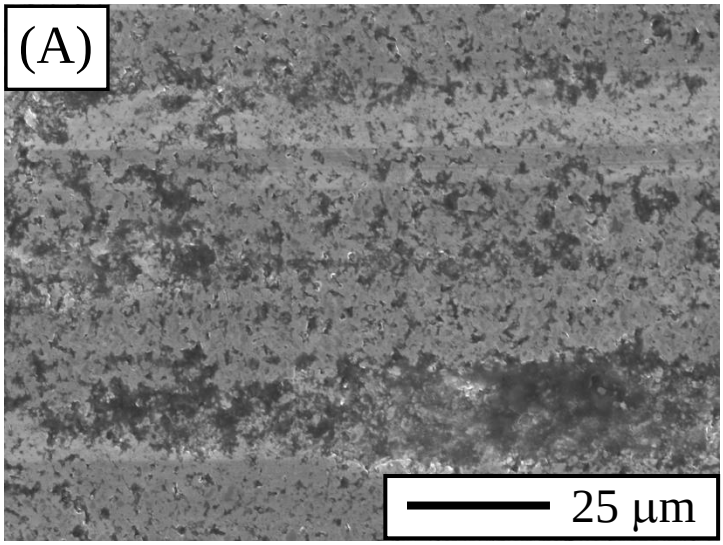

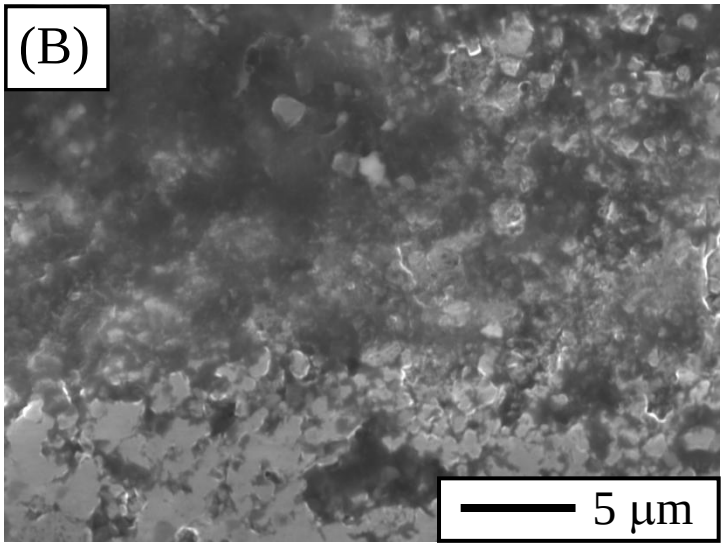

Ortiz *et al.*
Figure 4

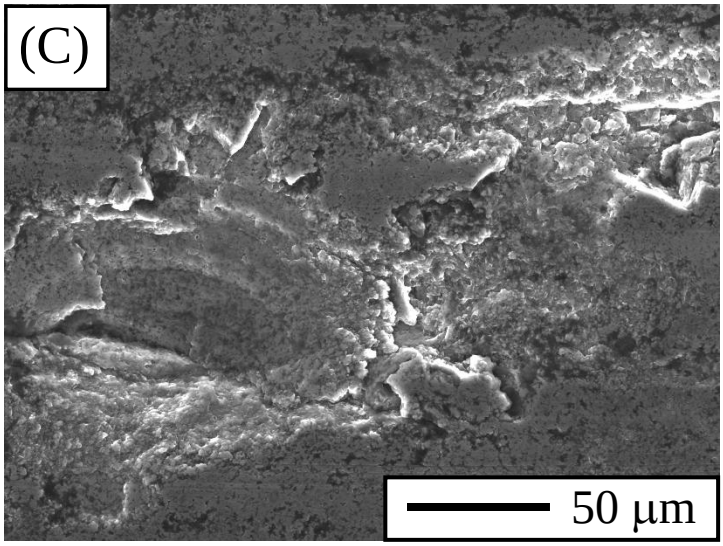

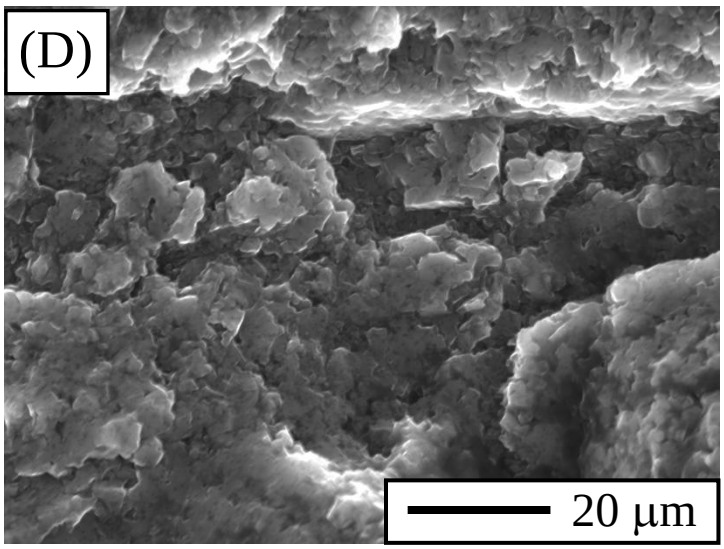

Ortiz *et al.*
Figure 4

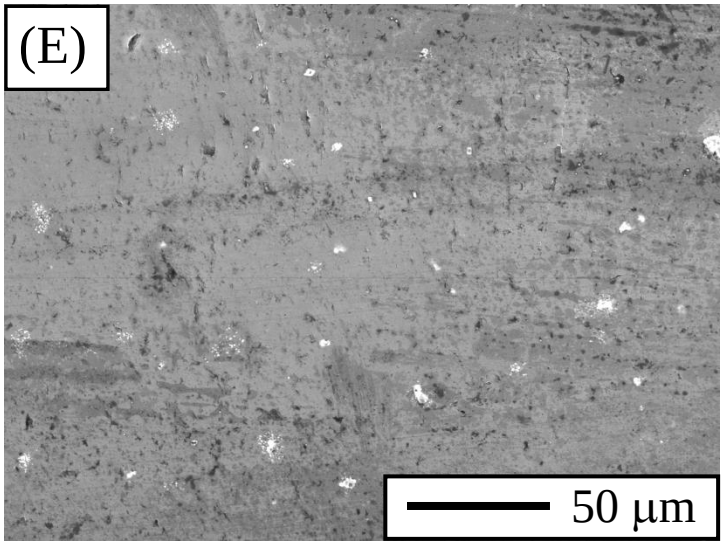

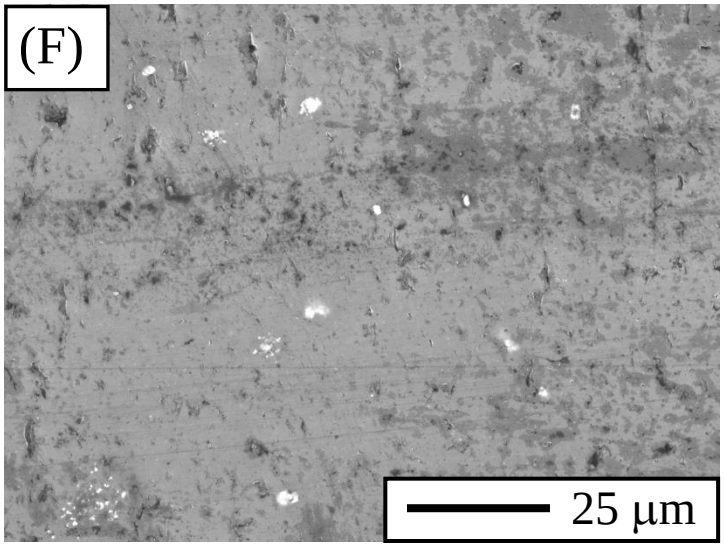

Ortiz *et al.*
Figure 4

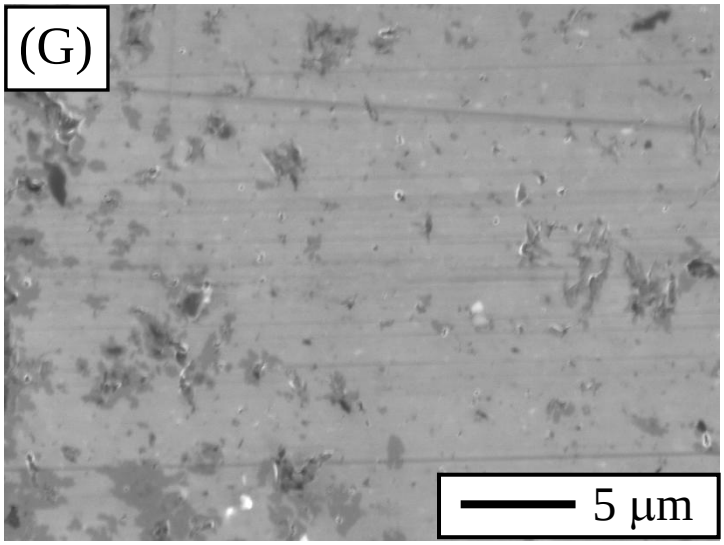

Ortiz *et al.*
Figure 4

Graphical Abstract